ELSEVIER

International Journal of Mass Spectrometry 215 (2002) 45–58

International Journal of Mass Spectrometry

www.elsevier.com/locate/ijms

Cryogenic detectors and their application to mass spectrometry

Hans Kraus

Department of Physics, University of Oxford, Keble Road, Oxford OX1 3RH, UK

Received 5 July 2001; accepted 5 October 2001

Abstract

Cryogenic detectors are detectors based upon detection mechanisms which require low temperatures in the sub-kelvin range, such as superconductivity. This article introduces the two main representatives of cryogenic detectors, superconducting tunnel junctions and low-temperature calorimeters with superconducting thermometers. The operating principles, signal generation and noise sources are discussed in each case. These detectors are already applied to experiments in particle-astrophysics and in optical astronomy. They are considered as the next generation instrumentation in certain areas of astrophysics, material analysis and high-resolution spectroscopy. Since 1996, they are also considered for applications in time-of-flight spectrometry of heavy bio-molecules. Successful applications of both detectors types in this area are briefly reviewed. (Int J Mass Spectrom 215 (2002) 45–58) © 2002 Elsevier Science B.V. All rights reserved.

Keywords: Detectors; Bolometer; Superconducting junctions; Mass spectrometry; Calorimeters

1. Introduction

Cryogenic detectors have been developed since the early 1980s for applications in particle physics, astrophysics and also for material analysis. The results are summarized in the proceedings of the low temperature detector (LTD) conference series [1–8]. The main motivations for their application in these fields were the vast improvement of spectral resolving power, which these detectors offer, and the possibility of having detectors with low energy thresholds and large sensitive absorber areas. Recently, time-of-flight mass spectrometry has been added to the list of applications. For this, the ability of detecting slow-moving massive particles with near 100% efficiency and the additional information gained from measuring the energies of the arriving bio-molecules are the main driving force.

Many conventional mass spectrometers use microchannel plates (MCPs) to measure the arrival time of molecules. Although MCPs are fast and easy to use, their detection of particles relies on secondary electron emission, which is inversely proportional to the velocity of the incoming molecules, making it increasingly difficult to detect heavy molecules with masses exceeding several tens of kDa. Detectors based on secondary ion emission, such as conversion dynodes, can be used to obtain good sensitivity at higher molecule masses, however their timing resolution is much worse than that of detectors based on secondary electron emission. Cryogenic detectors may be very suitable for detecting molecules of high mass and with good time resolution.

Molecules in time-of-flight mass spectrometers are accelerated to energies of typically 10–30 keV. Limitations to this energy may arise from the monitored charge states, the maximum acceleration voltage and

E-mail: h.kraus@physics.ox.ac.uk

PII S1387-3806(01)00546-2

the stability of the molecule. Cryogenic detectors are well positioned to detect these energies with high quantum efficiency as they operate at temperatures in the milli-kelvin range. The detection mechanism is based on the creation of phonons in dielectric absorbers or of quasi-particles in superconductors. The energies required for the creation of a single excitation are of the order of sub-meV and as the creation of these excitations does not involve ionization, the detection efficiency remains close to 100% even for very heavy molecules.

A significant advantage of cryodetectors is their ability of having excellent energy resolution in the energy range in question. This is useful in identifying different charge states of the intact molecule or its fragments. From time-of-flight measurements, the ratio m/z, where m is the mass of the molecule and z is the charge state can be determined. For example, singly charged monomers, doubly charged dimers and triply charged trimers have the same ratio m/z and thereby cannot be distinguished unless further information is available. As the kinetic energy of a molecule is proportional to its charge state z, the different charge states can be separated by using a detector with good energy resolution. Energy resolution also helps in identifying fragment ions, which are provoked by unimolecular and/or collision-induced dissociation within the mass spectrometer.

The following two sections introduce two types of cryogenic detectors, superconducting tunnel junctions and low-temperature calorimeters. Superconducting tunnel junctions utilize a similar concept as detectors based on semiconductors, namely the existence of an energy gap across which charge carriers or quasi-particles are excited. The number of thereby created excitations is proportional to the absorbed energy. As the effective energy gap in a superconductor is of order ∼meV as compared to ∼3 eV in semiconductors, the number of excitations created in superconductors is enhanced significantly with respect to semiconductors, supporting a substantial gain in resolving power and detection threshold. The other type of cryogenic detector, thermal detectors (bolometer and calorimeter), consists of an absorber in which the energy of a particle is converted into an increase of temperature. This temperature increase is measured by a temperature transducer. Among the more prominent examples are: semiconductor thermistors, such as neutron transmutation-doped germanium (NTD-germanium sensors), normalconductor–insulator–superconductor (NIS) tunnel junctions and superconducting phase transition thermometers (SPTs). Recently, NIS junctions have been applied to the spectroscopy of bio-molecules. In these sensors, electrons injected from the superconductor through the insulating tunnel barrier into the normalconductor heat the electrons therein. This increase of the electron temperature can be measured as a change of current through the NIS junction. Research on SPT sensors for application to the spectroscopy of bio-molecules is being intensified. Already for considerable time, SPT-based detectors have been applied in heavy ion physics [9]. The high sensitivity of SPTs is based upon the sharpness of the phase transition between the superconducting and normalconducting states of a superconductor. Biased within this transition, a change of the temperature of the electron system causes a change of electrical resistance which is measured by an external electronic readout circuit.

2. Superconducting tunnel junctions

Superconducting tunnel junctions consist of two thin films of superconductors, separated by a thin tunnel barrier through which quantum-mechanical tunneling of electrons can occur [10]. A typical geometry is shown in Fig. 1.

The tunnel current through the barrier is proportional to the number of quasi-particles in the superconducting tunnel junction (STJ). Such quasi-particles are created by liberating the two electrons normally bound in a Cooper pair and excitation across the superconducting energy gap. This can be caused either by thermal excitation or by energy available after absorption of an energetic particle. The amount of energy required to break a Cooper pair is 2Δ, Δ being the energy gap parameter of the superconductor (typically ∼meV).

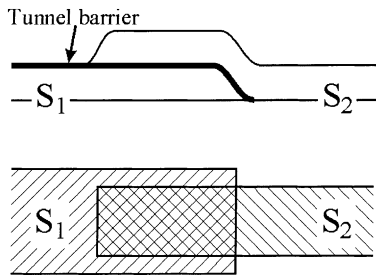

Fig. 1. The geometry of a superconducting tunnel junction is shown as a cross-section and as a top view. The two superconductors S_1 and S_2 are separated by a thin tunnel barrier. The overlap area, where tunneling is possible, has typical dimensions of 100 μm × 100 μm and the layer thicknesses are of order >200 nm.

However, since the particle energy to be measured is in general orders of magnitude higher than Δ, the energy is shared among other electrons in the material and by inelastic scattering, the number of excited electrons increases while their individual energy decreases [11]. Later in this energy cascade, electrons can lower their energy by emission of phonons. These phonons break Cooper pairs into two excited quasi-particles which in turn relax to the band gap, again emitting phonons. At energy levels close to the band gap it does matter whether the phonon still has energy above 2Δ, in which case it can produce further quasi-particles, or if its energy is lower than 2Δ, in which case the energy is lost. These are all statistical processes and the Fano factor F in combination with the effective energy gap Δ_{eff} accounts for this. The effective energy gap is in general 1.7 times the intrinsic energy gap and the Fano factor is usually of order 0.1–0.2 [12]. The energy resolution ΔE due to statistics of charge carriers is then

$$\Delta E = 2.36\sqrt{\Delta_{\mathrm{eff}} F E}. \tag{1}$$

2.1. The signal

After energy absorption in the STJ and the creation of an excess density of quasi-particles, the quasi-particles tunnel, thereby creating the signal, or they relax via loss processes without having contributed to the signal. The excess tunnel current I_{exc} resulting from the absorption of energy E is, in a simplified approach, modeled by an exponentially decaying current signal with fall time of $\tau_{\mathrm{P}} = 1/\gamma_{\mathrm{P}}$.

$$I_{\mathrm{exc}} = \frac{eE}{\Delta_{\mathrm{eff}}}\gamma_{\mathrm{T}} \exp(-\gamma_{\mathrm{P}} t),$$
$$Q_{\mathrm{t}} = \int_0^{\infty} I_{\mathrm{exc}}\, \mathrm{d}t \propto \frac{\gamma_{\mathrm{T}}}{\gamma_{\mathrm{P}}} E \tag{2}$$

where γ_{T} is the tunneling rate constant and γ_{P} the total loss rate constant for quasi-particles; e is the elementary charge. The signal of superconducting tunnel junction is ideally measured with an amplifier that measures current or charge, rather than voltage. Current measurements are predominantly used for precise timing measurement, as in time-of-flight spectroscopy, whereas charge measurement is preferred for spectrometry. In any case, the best result in terms of signal to noise ratio is achieved by aiming for a tunnel rate constant γ_{T} as high as possible while minimizing the loss rate γ_{P}. This is immediately obvious from Eq. (2) for the total charge Q_{t}. It is one of the aims in design and fabrication of tunnel junctions to achieve a maximized $\gamma_{\mathrm{T}}/\gamma_{\mathrm{P}}$.

2.2. The contributions to the rates γ_T and γ_P

Quasi-particle recombination $\gamma_R(T)$: This temperature-dependent loss term describes the recombination of two quasi-particles under formation of a Cooper pair and the subsequent escape of a recombination phonon. This loss process is proportional to the density of quasi-particles available for recombination. The density of thermally excited quasi-particles is

$$n_{\mathrm{therm}} \approx 2n_0\sqrt{2\pi\,\Delta k_{\mathrm{B}} T}\, \exp\left(-\frac{\Delta}{k_{\mathrm{B}} T}\right) \tag{3}$$

with n_0, k_{B}, and T the single spin density of states, Boltzman constant and operating temperature, respectively. Thus, by lowering the operating temperature T to less than ∼10% of the superconductor's characteristic temperature T_{C}, this thermal density and thereby γ_{R} becomes negligible. However, there remains the possibility that excess quasi-particles recombine with other excess quasi-particles. This process causes an energy-dependent loss process and gives rise to a

departure from the simple exponential pulse shape suggested in Eq. (2). It has the further consequence that high energy resolving power in STJs is more easily achieved for the detection of optical photons [13], while good energy resolution for the keV-energy range requires more elaborate STJ designs.

Quasi-particle loss γ_L: This temperature independent loss term can have a variety of causes. Less than optimum tunnel junction design can lead to quasi-particles diffusing out of the tunnel volume which diminishes the quasi-particle density available for tunneling. Another common problem is a potentially lower energy gap along the perimeter of an STJ, and when quasi-particles become trapped in these regions, they may become unable to contribute to the signal. Furthermore, surface roughness, trapped magnetic field, magnetic impurities and other causes, which effect a departure from the properties of an ideal bulk superconductor, decrease the density of quasi-particles which would normally contribute to the signal. In addition, γ_L is often non-uniform across the tunnel junction, thereby introducing a position-dependent response of the STJ. These temperature-independent loss processes were initially noted indirectly when the observation was made that the decay time of quasi-particles did not increase with lowering temperature as predicted by pair recombination alone. Detailed studies with a low temperature scanning electron microscope (LTSEM) by Hübener et al. at the University of Tübingen, Germany produced numerous important results regarding the signal generation and causes for quasi-particle losses in STJs [14,15]. The tunnel process itself may have to be counted as a loss process as well. Whether it needs to be included in the loss rate depends on the design of the STJ and in particular whether the quasi-particles have a chance to tunnel multiply.

Tunnel processes γ_T: The tunnel rates with which the quasi-particles transfer from one electrode of a tunnel junction to the other can be calculated using Fermi's Golden Rule. By using the density of states according to the BCS-theory and by assuming the normalconducting density of states n_0 near the Fermi energy to be constant, the tunnel rates γ_T are

$$\tau_{T_{L,R}} = \frac{1}{4e^2 n_0} \frac{1}{R_{NN} A d_{L,R}} \frac{\Delta + eV}{\sqrt{(\Delta + eV)^2 - \Delta^2}} \tag{4}$$

As the two metal films of a tunnel junction have in general different thicknesses d_L, d_R the tunnel rate constants are unequal for both films. The γ_{T_L} and γ_{T_R} are the tunnel rate constants for quasi-particles tunneling from left to right and from right to left, respectively (see Fig. 2). R_{NN} is the "normal conducting" resistance of the tunnel junction measured at voltages V well above $2\Delta/e$, and A is the area of the tunnel junction, where tunneling of quasi-particles is possible. Allowing for energy absorption in either of the two films the excess tunnel current I_{exc} is given by

$$I_{exc} = e(\gamma_{T_L} N_L + \gamma_{T_R} N_R) \tag{5}$$

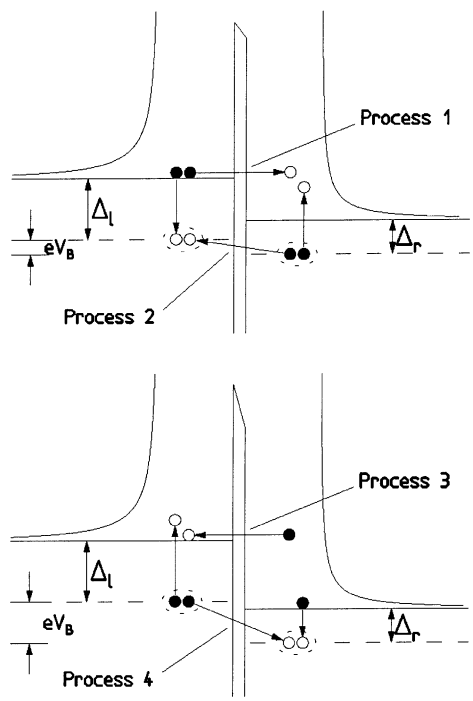

Fig. 2. The four different tunnel processes which occur in STJs. The upper diagram shows the situation for bias voltages $V_B < (\Delta_l - \Delta_r)/e$ and the lower for $V_B > (\Delta_l - \Delta_r)/e$. The vertical axes are energy scales and to the left and right, the BCS-densities of state are drawn. Full circles denote quasi-particles before they tunnel, open circles show the situation after the tunnel process.

N_L and N_R are the *numbers* of quasi-particles excited in the left and right layers in the area A of the tunnel junction. If an equal amount of energy is absorbed in either film of the tunnel junction, an equal *number* of quasi-particles results. Due to the inequality of the tunnel rate constants, the amplitudes of the current signals observed are dependent on the film in which the absorption took place. In tunnel junctions, where the ratios of $\gamma_{T_L}/\gamma_{P_L}$ and $\gamma_{T_R}/\gamma_{P_R}$ (cf. Eqs. (2) and (5)) are different, a doubling of the peak structure occurs. This has been shown in numerous publications, mainly for STJ tests with the X-ray photons produced by a ^{55}Fe source, giving out energies of 5.89 keV (88%) and 6.49 keV (12%) [1–8,16]. The two dominant tunnel processes in tunnel junctions with equal energy gaps $\Delta = \Delta_l = \Delta_r$, responsible for this feature, can be identified as processes 1 and 4 in Fig. 2. Both processes 1 and 4 lead to a unidirectional flow of electrical current and the polarity of the signal is independent of whether the excess quasi-particle density was generated in the left or in the right layer of the STJ.

In tunnel junctions with electrodes of unequal energy gaps ($\Delta_l \neq \Delta_r$) an important consequence for detector applications is that the tunnel rate constant may be much smaller than expected or even be negative. Fig. 2 shows the various tunnel processes possible in such STJs. Since excited quasi-particles relax to the gap edge within a very short time and since the operating temperature is assumed to be very low, the simplification of quasi-particles occupying exclusively states with energies of the energy gap (i.e., Δ_l and Δ_r) can be made. In reality, where the distribution of quasi-particles is different from a δ-like distribution (e.g., Fermi–Dirac distribution function for thermal excitation), the statements made here still hold in general, but become less stringent due to the presence of excited quasi-particles [17]. The different tunnel processes are

Process 1 is possible for all positive bias voltages. It causes an electron current from left to right and with respect to the applied voltage a positive electrical current. The density of final states of the right layer into which the quasi-particles tunnel is a function of the applied bias voltage. The tunnel rate constant is maximum at zero voltage and reduces with increasing voltage.

Process 2 is only possible for voltages lower than $V_B < (\Delta_l - \Delta_r)/e$. It causes an electron current from right to left and thus, a negative electrical current. The maximum negative current is obtained for a bias voltage equal to $(\Delta_l - \Delta_r)/e$. This negative current can easily exceed the positive current since the density of final states for this process can be much higher than for process 1. The combination of processes 1 and 2 yields a total negative electrical current in the bias voltage range $0 < V_B < (\Delta_l - \Delta_r)/e$ since the density of final states in the right electrode for process 2 is always higher than for process 1. At bias voltages $V_B > (\Delta_l - \Delta_r)/e$ process 2 is forbidden and the negative component of the electrical tunnel current vanishes. The total current is again positive.

Process 3 is strongly suppressed and will be neglected. It would require highly excited quasi-particles in the right layer.

Process 4 is the equivalent to process 1, only that it applies to quasi-particles in the right layer. These quasi-particles could result from energy absorption in the right layer or from quasi-particles having tunneled previously via process 1 or 2. It provides a possibility for repeated tunneling of quasi-particles.

In tunnel junctions with equal energy gaps, processes 2 and 3 are highly suppressed and only processes 1 and 4 are considered. The combination of processes 1 and 4 allows quasi-particles to tunnel repeatedly as long as they are present in the tunnel volume. This mechanism leads to an intrinsic signal amplification and was experimentally shown by Gray [18]. As long as provisions are made to confine the quasi-particles to the tunnel volume, they can tunnel repeatedly and tunneling is not a loss process. However, if the layer into which the quasi-particles tunnel is, e.g., a large wiring layer allowing them to readily escape from the tunnel volume, then tunneling has to be counted as loss process. Processes 2 and 3 are only possible if the quasi-particles in the electrode from which they originate are excited above the energy gap or if they occupy a higher energy level due to a larger energy gap, a situation found in STJs with

$\Delta_l \neq \Delta_r$. Such heterojunctions are created whenever bilayer, e.g., from aluminum and niobium are used to form the two electrodes of the tunnel junction. Designs with two bilayer may be used to form proximity layers for both electrodes in order to concentrate the quasi-particles near the tunnel barrier and to enhance the signal by multiple tunneling. One would aim for as similar as possible bilayer and the situation then would be more like in a tunnel junction with equal energy gaps.

An example for the high resolving power achieved with superconducting tunnel junctions is shown in Fig. 3. Angloher et al. used STJs made of aluminum on a silicon-nitride (Si_3N_4) membrane [19]. The membrane of thickness 300 nm, in contrast with a solid substrate, improves the performance of the STJ detector significantly. Contributions from absorption in the substrate can be neglected. In solid substrates, these normally cause a continuum of signal amplitude, strongly dependent on how many phonons from the substrate reach the STJ. Early attempts to avoid this feature employed buffer layers [20,21], but the availability of membranes has simplified the detector fabrication process. The membrane also helps reducing quasi-particle losses as recombination phonons escaping the STJ may be reflected at the backside of the membrane and be re-absorbed by the STJ. A 1.3 μm thick lead absorber has been deposited with the principal aim of increasing the quantum efficiency for X-ray absorption compared with a thin layer of aluminum. As can be seen in Fig. 3, the quantum efficiency of the lead layer is so high for 6 keV X-ray photons that the usual problem of having different responses from the two layers of an STJ is no longer present. The lead absorber is not in metallic contact with the aluminum of the top STJ layer. If that was the case, proximity

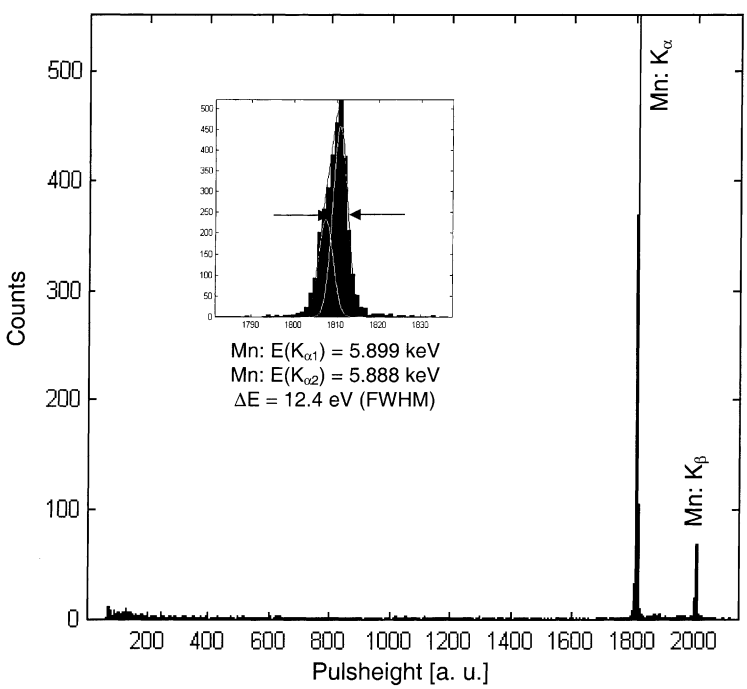

Fig. 3. Energy spectrum obtained for irradiation of an aluminum STJ of area 100 μm × 100 μm with X-ray photons of 5.89 and 6.49 keV. The STJ was fabricated on a Si_3N_4 membrane and was equipped with a Pb absorber (90 μm × 90 μm, 1.3 μm thickness) deposited onto the top aluminum layer of the STJ. X-ray photons are absorbed in the Pb whereby the doubling of peak structure usually present in STJs has been avoided. Courtesy of G. Angloher, University of Oxford, formerly Technische Universität München, Germany.

effect would alter the energy gap of that film, thereby causing the problems of reduced signal currents as discussed above [17,22].

2.3. The noise

Good energy resolution and the capability of accurate timing of the arrival of particles require a high signal to noise ratio $\mathfrak{R}_{SN}$. A detailed discussion of noise in STJs is given in [22].

Energy E absorbed in an STJ produces initial charge carriers with a total charge $Q_t = e \times E/\Delta_{eff}$. Subjected to diffusion, recombination and other loss processes, only a fraction of this charge, Q_t, tunnels and contributes to the current signal. The tunnel current is measured using suitable front-end electronics and filter amplifiers (or software filters). At the output of this electronics chain, a voltage, proportional to the charge Q_t is present, but also electronic noise. As explained in more detail in [22], the spectral density of the signal is given by $Q_t \times S(\omega)$ and $\mathcal{N}(\omega)$ is the spectral power density of the noise. The highest possible signal to noise ratio $\mathfrak{R}_{SN}$ is achieved by application of the optimum filter.

$$\mathfrak{R}_{SN} = \left(\frac{1}{2\pi} \int \frac{Q_t^2 S^2(\omega)}{\mathcal{N}(\omega)} \, d\omega \right)^{1/2}. \quad (6)$$

The signal $Q_t \times S(\omega)$ is the product of the Fourier transform of the excess tunnel current $I_{exc}(\omega)$ and the transfer function of the readout system $P(\omega)$. The tunnel current in the time domain is given in Eq. (2). Noise under omission of $1/f$ noise is given by

$$\mathcal{N}(\omega) = \left(\langle i_n^2 \rangle + \langle e_n^2 \rangle \left(\frac{1}{R_D^2} + \omega^2 C_i^2 \right) \right) P^2(\omega). \quad (7)$$

where $\langle e_n^2 \rangle$ and $\langle i_n^2 \rangle$ are the voltage and current noise sources situated in series and parallel to the detector, respectively. R_D is the dynamical resistance of the detector at the bias point and C_i is the capacitance present at the input of the preamplifier. In general, STJ detectors are read out by amplifiers based on JFETs as the input device, which is most appropriate for the high values of R_D achieved in good quality STJs. In this case, series noise $\langle e_n^2 \rangle$ arises mainly from fluctuations in the channel of the input FET of the readout system while parallel noise $\langle i_n^2 \rangle$ has several origins:

$$\langle e_n^2 \rangle = 4k_B T \frac{0.65}{g_m} \quad (8a)$$

$$\langle i_n^2 \rangle = 2e(I_d + I_g) + 4k_B T (R_B^{-1} + R_F^{-1}) \quad (8b)$$

where T is the temperature of the junction in the FET and g_m is the forward transconductance of the FET. I_d and I_g are the detector and FET gate leakage currents and R_B, R_F are the load and feedback resistors. In an optimum experimental setup, the parallel noise contributions introduced by electronics can be made negligible compared to the detector leakage current I_d which is related to the quality of the tunnel junction. The optimal signal to noise ratio $\mathfrak{R}_{SN}$ in terms of parameters of the STJ and as a function of energy E is

$$\mathfrak{R}_{SN} = \frac{\tau_p}{\tau_T} \frac{eE}{\Delta_{eff}} \frac{1}{\sqrt{\langle i_*^2 \rangle (\tau_s + \tau_p)}} \quad (9)$$

with $\langle i_*^2 \rangle = \langle i_n^2 \rangle + \langle e_n^2 \rangle / R_D^2$ the effective parallel noise, $\tau_s = 2(\langle e_n^2 \rangle / \langle i_*^2 \rangle)^{1/2} C_D$ the optimal filtering time in case of a CR-RC shaper, and $\tau_T = 1/\gamma_T$ is the inverse tunnel rate. The pulse length $\tau_p = 1/\gamma_p$ is a critical parameter, because it affects *both* signal charge and equivalent noise charge.

The optimization parameter for tunnel junctions are essentially such that the tunneling time τ_T should be as short as possible, while the quasi-particle lifetime τ_P should be long. The leakage currents should be small and the ratio of the dynamical resistance R_D at the operating voltage to the normalconducting resistance R_{NN} should be maximized. These parameters are only in part determined by the fabrication process. For example, τ_T is a function of bias voltage (see Eq. (4)). But so is R_D; in addition R_D depends on the amount of trapped magnetic flux within the STJ. R_D reduces with increased trapped flux and lower R_D translates into higher electronic noise. Such trapped flux can be introduced through a variety of processes, most notably, external electromagnetic interference or mechanical vibration. Warming an STJ to temperatures above the critical temperature of the superconductor

expels such flux and after cooling of the STJ to the operating temperature, R_D is normally restored to its initial high value.

2.4. STJs used in mass spectrometry

STJ technology has matured, but as outlined above, the use of such technology to obtain operation for optimum results may require experience somewhat beyond that of the non-expert. STJs applied to mass spectrometry are used by the groups at Neuchatel/Paul Scherrer Institute, Switzerland [22] and at Lawrence Livermore National Laboratory (LLNL), USA [23]. An early review on this subject was written by Booth [26,27]. The application of STJs to mass spectrometry was pioneered by Twerenbold et al. who used STJs based on tin [24]. Tin STJs of area 20 μm × 80 μm were operated at a temperature of ∼0.4 K in a ^{3}He cryostat attached to a custom-built MALDI-TOF system. In these initial experiments, individual lysozyme molecules (14,300 Da) as well as DNA oligonucleotides were detected [26]. The tin STJs were read out with charge sensitive preamplifiers. Pulse shaping with a time constant of $\tau = 500$ ns was applied before the pulse trace was recorded with a waveform analyzer. The time-of-flight of the molecules was determined from the time difference between the onset of the signal associated with the arrival of the molecule and the signal produced by absorption of the UV light of the laser pulse used to desorb molecule–ions from their matrix in the source. Tin STJs were only used for initial demonstration experiments. Tin is a soft material that has a strong tendency to grow whiskers. As a consequence, the quality of such STJs may degrade after repeated thermal cycling between room temperature and the operating temperature in the sub-kelvin region.

More recently, the group started to use STJs based on aluminum, which seems to be the best material known to date for high quality STJ fabrication. The aluminum STJs had an area of the tunneling region of 50 μm × 400 μm. The results obtained for immunoglobulin G (IgG, 145 kDa) were reported in [28]. Fig. 1 therein shows the comparison of the results obtained with a detector measuring ion currents and an aluminum STJ.

The LLNL group applied Nb–Al_2O_3–Nb tunnel junctions to mass spectrometry [29]. They measured the spectra of the human serum albumin (HAS, 66.3 kDa) and of IgG (150 kDa). In addition to the time of flight information, they used the information on the energy carried by the molecules to distinguish the various charge states of the ions [25].

3. Low-temperature calorimeters

Fig. 4 shows the typical components of a thermal detector which consists of an absorber for radiation or particles, a temperature transducer which measures the temperature $T(t)$ of the absorber which is normally at its equilibrium temperature T_0 and a thermal link to a constant temperature reservoir T_B with differential heat conductance g.

The following derivation of the detector signal assumes immediate thermalization of the phonons and electrons in the absorber and thermometer and treats absorber and thermometer as infinitely well coupled to

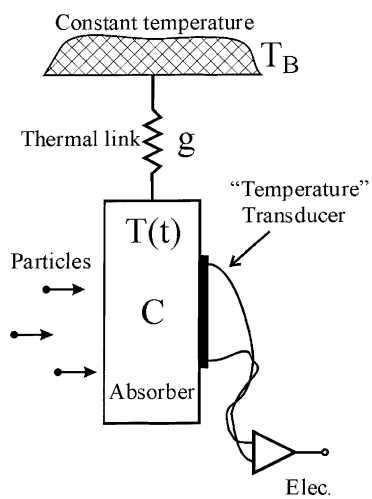

Fig. 4. The principal components of a thermal detector (calorimeter or bolometer) are the absorber with heat capacity C which absorbs particles or radiation, the temperature transducer which transforms temperature changes into electrical signals and the thermal link g to a reservoir of constant temperature T_B.

each other. This is of course a very simplified picture but it is adequate to show the general features of thermal detectors. A more elaborate treatment, especially taking decoupling of the electron and phonon systems at very low temperatures into account, was carried out by Pröbst et al. [30].

Thermal detectors are often termed bolometer or calorimeter. To name a detector "bolometer" is more appropriate if the time interval between the absorption of individual particles is much shorter than the intrinsic time constant of the detector. Then, the energy flux or the power of the incident radiation is measured. If, by contrast, the interval between the arrivals of individual particles is much longer than the detector time constant and the energy of the individual particles is measured then the detector is a calorimeter.

The work on bolometer and calorimeter is well reviewed in articles, especially on such devices for infrared and millimeter waves [31], low-T_C bolometer [32] and including high-T_C bolometer [33–35]. Bolometer for infrared and optical radiation are summarized in [36] and a recent overview including the calorimetric aspect is given in [37].

3.1. The signal

The responsivity S of a thermal detector is the change in current or voltage across the temperature transducer as a response to a change in input power. Depending on whether current or voltage changes are measured, the current responsivity S_I or the voltage responsivity S_V is of interest. These are defined as

$$S_I = \frac{\partial I}{\partial P_{ext}} = \alpha R_0 \frac{\partial(\Delta T)}{\partial P_{ext}} \frac{\partial I}{\partial R} \tag{10a}$$

$$S_V = \frac{\partial V}{\partial P_{ext}} = \alpha R_0 \frac{\partial(\Delta T)}{\partial P_{ext}} \frac{\partial V}{\partial R} \tag{10b}$$

with P_{ext} the power input to the detector caused by external radiation or absorption of energetic particles. ΔT is the temperature change of the detector as sensed by the temperature transducer. This temperature transducer is considered to be a device which transforms a change in temperature into a change in resistance $R(T)$. For small temperature changes, R is given by

$$R \approx R_0 + \left.\frac{\partial R}{\partial T}\right|_{T_0} \Delta T = R_0(1 + \alpha\,\Delta T) \text{ with } \alpha = \frac{1}{R_0}\left.\frac{\partial R}{\partial T}\right|_{T_0} \tag{11}$$

thereby defining the temperature coefficient α. R_0 and T_0 are the resistance and temperature in the absence of P_{ext}. Superconducting phase transition (SPT) sensors are of particular interest because they can exhibit very high values of α owing to the steepness of the transition between the superconducting and normal-conducting phases (see Fig. 5).

For the calculation of $\partial(\Delta T)/\partial P_{ext}$, the equation for power flow in the detector has to be considered:

$$CT = \eta P_{ext} - P_{link} + P_{elec} \tag{12}$$

with C is the heat capacity of the detector, T its temperature, η the absorbance and P_{ext}, P_{link} and P_{elec} the power introduced by external radiation onto the detector, the power transfer between the detector and the constant temperature bath T_B and the power dissipation caused by the measurement current through

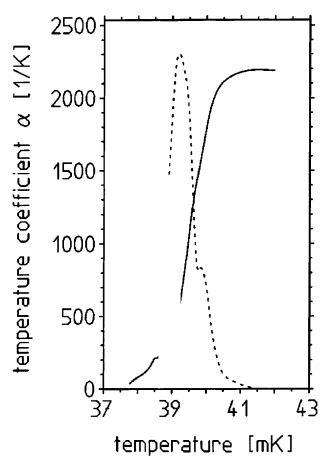

Fig. 5. Superconducting phase transition thermometer. The solid curve is the resistance versus temperature characteristics of an iridium–gold bilayer. The dashed curve is the temperature coefficient α, which exhibits a maximum at $T \simeq 39.5$ mK. Courtesy of J. Höhne of the Technische Universität München, Germany.

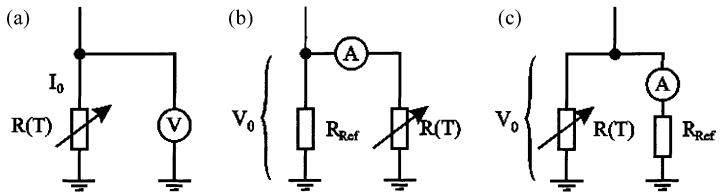

Fig. 6. Different modes of read-out for temperature transducers. The temperature transducer is shown as a temperature-dependent resistor $R(T)$. (a) Constant current, (b) constant voltage, and (c) constant power read-out. In (a), voltage changes are measured, while for (b) and (c) changes in current are measured.

the temperature transducer. In case of a calorimeter, which detects single particles (bio-molecules), each with energy E_i and arriving at time t_i, the external input power becomes $P_{\text{ext}}(t) = \sum_i E_i \times \delta(t - t_i)$. P_{link} can be expanded for small ΔT as

$$P_{\text{link}} = K(T^m - T_{\text{B}}^m) \approx \underbrace{K(T_0^m - T_{\text{B}}^m)}_{P_0} + \underbrace{mKT_0^{m-1}}_{g}\underbrace{(T - T_0)}_{\Delta T} \tag{13}$$

with K a material constant of the link and m the power of the temperature dependence of the heat conductance. Assuming that in the steady state, the sole power input results from the measurement current alone, P_0, g, and ΔT can be defined according to Eq. (13). The electrical power expanded in a similar way gives

$$P_{\text{elec}} \approx P_0 + \left.\frac{\partial P}{\partial T}\right|_{T_0} \Delta T \tag{14}$$

Inspection of Eq. (14) shows that the electrical power input caused by the measurement current is not necessarily constant. A variation of P_{elec} with ΔT gives rise to electrothermal feedback and its strength is governed by the value $\partial P/\partial T$. The sign and magnitude of this quantity and of $\partial I/\partial R$ and $\partial V/\partial R$, respectively, depends on the configuration of the electrical readout circuit and the detector bias scheme. Three different schemes are shown in Fig. 6 and their influence on detector relevant parameters is compiled in Table 1.

Using Eqs. (12)–(14), the equation for the temperature change ΔT rewrites as

$$C\Delta T + g\left(1 - \frac{1}{g}\left.\frac{\partial P}{\partial T}\right|_{T_0}\right)\Delta T = \eta P_{\text{ext}} \tag{15}$$

The responsivities (S_{V} for Fig. 6a and S_{I} for Fig. 6b and c) then assume the form of a low-pass with S_0 the zero-frequency responsivity and τ_{eff} the characteristic time constant.

$$S = S_0 \frac{1}{1 + i\omega\tau_{\text{eff}}} \tag{16}$$

Constant current readout (Fig. 6a), where the voltage drop across the temperature transducer is measured, increases its zero-frequency responsivity S_0 with increasing loop gain but its time constant becomes longer as well. If $\mathcal{L} \geq 1$, 'thermal runaway" occurs, a condition to be avoided. In the context of voltage bias (Fig. 6b) $\mathcal{L}$ is called the "loop gain" of the feedback loop. This feedback is caused by a power change P_{elec} as a result of a temperature change of the thermometer. "Extreme electrothermal feedback" [38–41] or ETF is achieved for $\mathcal{L} \gg 1$. Then, in constant voltage

Table 1
Zero-frequency responsivity and time constant for three difference bias modes

	Constant current	Constant voltage	Constant power
$(\partial P/\partial T)\|_{T_0}$	$+\alpha P_0$	$-\alpha P_0$	0
S_0	$(\eta/I_0)\cdot\mathcal{L}/(1-\mathcal{L})$	$(-\eta/V_0)\cdot\mathcal{L}/(1+\mathcal{L})$	$(\eta/2V_0)\mathcal{L}$
τ_{eff}	$\tau_0/(1-\mathcal{L})$	$\tau_0/(1+\mathcal{L})$	τ_0

$\tau_0 = C/g$ is the intrinsic time constant and $\mathcal{L} = \alpha P_0/g$.

mode as shown in Fig. 6b, S_0, the zero-frequency responsivity tends towards $-V_0^{-1}$ and is constant, which simplifies device operation. But what is much more important is the shortening of the time constant τ_{eff}. The effective time constant decreases by a factor $(1+\mathcal{L})^{-1}$ which permits higher counting rates in spectrometric applications and helps improve the energy resolution if the detector is operated as a calorimeter for single particle detection [38,40,42]. In constant power mode (Fig. 6c), the time constant does not change with read-out power and thermal runaway does not happen. The zero-frequency responsivity, however, can still be tuned to match experimental requirements.

3.2. Noise

A detector does not only produce an output signal in response to the absorption of radiation or particles. There are always fluctuations which cause noise and therefore impose a limit on the accuracy with which the signal can be measured. The minimization of noise is a very important issue in detector design and subsequent fabrication. The various noise sources in bolometer are extensively discussed in the literature [43]. The noise equivalent power NEP is the power input which produces the same detector output as the noise of the detector. All noise sources contributing to NEP are referred to the same point in the detector system, the external power input here and optimum filtering of the detector output is assumed. The following is a summary of the most common noise sources in bolometer and calorimeter:

Thermal noise: Energy fluctuation between the detector and the temperature reservoir across the thermal link is often referred to as phonon noise. Considering a detector with total heat capacity C and a thermal link with heat conductance g, a fluctuation of the energy contents of the absorber is caused by the random movement of energy carriers through the thermal link. An elementary result of classical statistical mechanics gives the mean square magnitude of the energy fluctuations [44]: $\langle \Delta E^2 \rangle = k_{\text{B}} T_0^2 C$, where T_0 is the operating temperature of the detector. This classical thermodynamic treatment assumes an equilibrium distribution of phonons. However, in reality, the phonon spectrum may be athermal and corrections must be made [30,36]. This noise source is an important limit for the sensitivity of a thermal detector. The fluctuation of energy exchange due to random propagation of energy carriers need not be restricted to phonons. Energy may also be exchanged by electrons, photons, or quasi-particles. The temperature dependencies of these thermal links are

$$g \propto \begin{cases} T^3 & \text{phonon exchange (insulator)} \\ T^3 & \text{phonon exchange (vacuum)} \\ T & \text{electron exchange (conductor)} \\ \exp(-\Delta/kT) & \text{quasi-particle exchange (superconductor)} \end{cases} \tag{17}$$

A commonly neglected noise source is caused by a temperature fluctuation of the temperature reservoir due to boiling cryogenics. Such fluctuations can be greatly minimized by the introduction of a large heat capacity with a long time constant to buffer the temperature reservoir to the detector.

Photon noise: Not only the exchange of heat across the thermal link causes noise. Also photons radiated from the detector and those impinging on it carry energy. Radiative exchange of energy takes place with the environment of the detector, e.g., the walls of the enclosure. This noise source can be neglected if the surroundings of the detector is cooled sufficiently. A noise source which cannot be avoided arises from background radiation in front of which a radiative source is to be observed. In the case of TOF mass spectrometry, this may be a serious limitation as the detector cannot be fully enclosed by walls at very low temperature. The bio-molecules have to reach the detector and, unless sophisticated designs are used, the detector will face some small surface at higher temperature. This may limit the energy resolution of the detector.

Amplifier and load noise: Amplifier noise is always present. But in most applications its contribution can be made negligibly small by proper impedance matching, by cooling of electronic components and by

increasing the responsivity $|S|$ of the detector. A load resistor R_L for biasing the thermometer also contributes Johnson noise. This noise is usually made negligible by using a value for R_L much higher than the thermometer resistor ($R_L \gg R_0$) and by cooling to very low temperature.

3.3. Application of calorimeters

Low-temperature calorimeters have been mainly developed for X-ray astrophysics, material analysis, nuclear spectroscopy and dark matter searches [1–8]. The highest resolving power of $E/\Delta E = 1300$ at 6 keV energy has been reported by Hilton et al. [45]. They used a superconducting phase transition thermometer (cf. Fig. 5) on a Si_3N_4 membrane to detect the X-rays emitted from a ^{55}Fe source. At an energy of 5.89 keV, the energy resolution is 4.5 eV. The thermometer was made from a molybdenum–copper bilayer, resulting in an operating temperature of 0.23 K. An individual detector element has an active area of 0.4 mm × 0.4 mm, significantly greater than that of STJ detectors.

Detectors with sensors based on superconducting phase transition thermometers are best read out by Superconducting Quantum Interference Device (SQUIDs) owing to their low electrical impedance. In order to increase the active area of detectors such as the one reported in [45], SQUID multiplexers are being developed to read out large arrays of such detectors [46]. An example for the enormous absorber size that can be achieved with cryogenic detectors while still providing good energy resolution, Fig. 7 shows the energy spectrum obtained with a 262 g sapphire absorber and an SPT based on tungsten. These massive detectors are used by the CRESST collaboration [47] in searches for dark matter in the Universe. These two extremes, very high energy resolution and very large mass, demonstrate the potential of calorimetric low-temperature detectors.

In an application to mass spectrometry, Hilton et al. used a microcalorimeter consisting of a 200 μm × 200 μm silver absorber on a Si_3N_4 membrane. The thermometer was a hot-electron NIS tunnel junction thermometer [48]. Their experiments show impressively how different charge states of molecules can be identified, adding another dimension to the usual m/z axis.

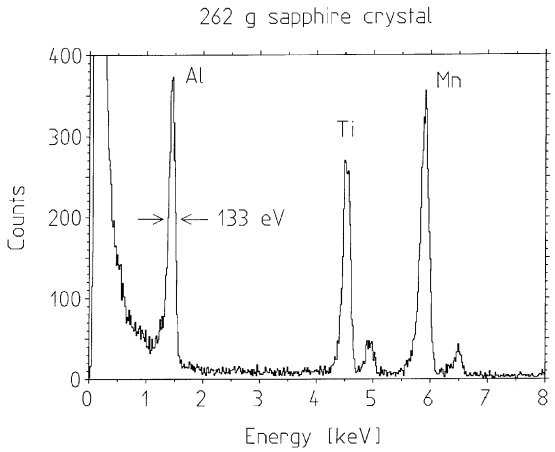

Fig. 7. Energy spectrum for various X-ray energies obtained with a 262 g sapphire detector as used in the CRESST dark matter search experiment and operated in active feedback mode. The sapphire absorber is a cube 4 cm at each side.

4. Summary

Cryogenic detectors have been seriously developed since the early 1980s. The 1990s have seen already a number of successful applications. In 1996, spectrometry of heavy bio-molecules was added to this list, and since then these experiments with superconducting tunnel junctions as well as with low-temperature calorimeters have been carried out. Cryogenic detectors offer high detection efficiency up to several 100 kDa, but even more important, their very good energy resolution offers much increased information on charge state, fragmentation, etc. The noise and some other processes that limit the energy resolution of cryodetectors seem to be reasonably well understood for the absorption of X-rays and optical photons. Energy resolutions close to the theoretical limit have been demonstrated. However, the energy resolution achieved for the spectrometry of heavy bio-molecules is far worse than the theoretical limit. Exploring the reasons for this will be necessary as this may limit the

usefulness of cryogenic detectors for spectrometry of bio-molecules.

Cryogenic detectors operate at low temperatures, typically near 100 mK, or even much lower, which requires coolers (cryostats) to provide this low-temperature environment. The traditional method of achieving these low temperatures involves liquid helium and nitrogen, which is not always feasible. There are developments of "cryogen-free" cooler systems, and the commercialization does not appear far away. Such systems could render the operation of cryogenic detectors very user-friendly [49,50]. It seems that in the near to mid-term future, the prime application of cryogenic detectors in this area will be in fundamental research and as a diagnostic tool for time-of-flight mass spectrometry.

References

[1] K. Pretzl, N. Schmitz, L. Stodolsky (Eds.), Low Temperature Detectors for Neutrinos and Dark Matter, Springer, Berlin, 1987.
[2] L. Gonzales-Mestres, D. Perret-Gallix (Eds.), Low Temperature Detectors for Neutrinos and Dark Matter II, Editions Frontières, Gif-sur-Yvette, France, 1988.
[3] L. Brogiato, D.V. Camin, E. Fiorini (Eds.), Low Temperature Detectors for Neutrinos and Dark Matter III, Editions Frontières, Gif-sur-Yvette, France, 1989.
[4] N.E. Booth, G.L. Salmon (Eds.), Low Temperature Detectors for Neutrinos and Dark Matter IV, Editions Frontières, Gif-sur-Yvette, France, 1992.
[5] S.E. Labov, B.A. Young (Eds.), The Fifth International Workshop on Low Temperature Detectors, J. Low Temp. Phys. 93 (1993) 185–858.
[6] H.R. Ott, A. Zehnder (Eds.), Low Temperature Detectors (LTD-6), Nucl. Instr. Meth. A 370 (1996) 1–300.
[7] S. Cooper (Ed.), in: Proceedings of the Seventh International Workshop on Low Temperature Detectors LTD-7, Max-Planck-Institute of Physics, 1997, ISBN 3-00-002266-X, available from urg@mppmu.mpg.de
[8] P. De Korte, T. Peacock (Eds.), in: Proceedings of the 8th International Workshop on Low Temperature Detectors (LTD-8), Nucl. Instr. Meth. A 444 (2000) 3–514.
[9] H.J. Meier, P. Egelhof, W. Henning, A. von Kienlin, G. Kraus, A. Weinbach, Nucl. Phys. A 626 (1997) 451C.
[10] I. Giaever, H.R. Hart, K. Megerle, Phys. Rev. 126 (1962) 941.
[11] C.A. Mears, S.E. Labov, M. Frank, M.A. Lindeman, L.J. Hiller, H. Netel, A.T. Barfknecht, Nucl. Instr. Meth. A 370 (1996) 53.
[12] M. Kurakado, Nucl. Instr. Meth. 196 (1982) 275.
[13] N. Rando, P. Verhoeve, A. van Dordrecht, A. Peacock, M. Perryman, S. Andersson, J. Verveer, B. Collaudin, D.J. Goldie, R. Venn, Nucl. Instr. Meth. A 370 (1996) 85.
[14] R. Gross, T. Doderer, R.P. Hübener, F. Kober, D. Kölle, C. Krülle, J. Man n hart, B. Mayer, D. Quenter, A. Ustinov, Physica B 169 (1991) 415.
[15] J.B. le Grand, M.P. Bruijn, C. Patel, P.A.J. de Korte, S. Lemke, R. Gross, R.P. Huebener, Physica C 279 (1997) 85.
[16] P. Hettl, G. Angloher, F.v. Feilitzsch, J. Höhne, J. Jochum, H. Kraus, R.L. Mössbauer, in: Proceedings of the Conference EDXRD-98, Bologna, X-ray Spectrometry 28 (1999) 309.
[17] H. Kraus, M. Gutsche, P. Hettl, J. Jochum, B Kemmather, J. Supercond. 9 (1996) 245.
[18] K.E. Gray, Appl. Phys. Lett. 32 (1978) 392.
[19] G. Angloher, P. Hettl, M. Huber, J. Jochum, F.v. Feilitzsch, R. L Mössbauer, J. Appl. Phys. 89 (2001) 1425.
[20] G. Angloher, B. Beckhoff, M. Bühler, F.v. Feilitzsch, T. Hertrich, P. Hettl, J. Höhne, M. Huber, J. Jochum, R.L. Mössbauer, J. Schnagl, F. Scholze, G. Ulm, Nucl. Instr. Meth. A 444 (2000) 214.
[21] W. Ootani, T. Ikeda, H. Kato, K. Kawai, H. Miyasaka, T. Oku, C. Otani, H. Sato, H.M. Shimizu, Y. Takizawa, H. Watanabe, H. Nakagawa, H. Akoh, M. Aoyagi, T. Taino, Nucl. Instr. Meth. A 444 (2000) 249.
[22] R. den Hartog, A. Golubov, D. Martin, P. Verhoeve, A. Poelaert, A. Peacock, M. Krumrey, Nucl. Instr. Meth. A 444 (2000) 28.
[23] J. Jochum, H. Kraus, M. Gutsche, B. Kemmather, F.v. Feilitzsch, R.L. Mössbauer, Nucl. Instr. Meth. A 338 (1994) 458.
[24] D. Twerenbold, Nucl. Instr. Meth. A 370 (1996) 253.
[25] W.H. Benner, D.M. Horn, J.M. Jaklevic, M. Frank, C.A. Mears, S.E. Labov, A.T. Barfknecht, J. Am. Soc. Mass Spectrom. 8 (1997) 1094.
[26] N.E. Booth, Rapid Comm. Mass Spectrom. 11 (1997) 944.
[27] D. Twerenbold, J.-L. Vuilleumier, D. Gerber, A. Tadsen, B. van den Brandt, P.M. Gillevet, Appl. Phys. Lett. 68 (1996) 3503.
[28] G. Gervasio, D. Gerber, D. Gritti, Y. Gonin, D. Twerenbold, J.-L. Vuilleumier, Nucl. Instr. Meth. A 444 (2000) 389.
[29] M. Frank, C.A. Mears, S.E. Labov, W.H. Benner, D. Horn, J.M. Jaklevic, A.T. Barfknecht, Rapid Commun. Mass Spectrom. 10 (1996) 1946.
[30] F. Pröbst, M. Frank, S. Cooper, P. Colling, D. Dummer, P. Ferger, G. Forster, A. Nucciotti, W. Seidel, L. Stodolsky, J. Low Temp. Phys. 100 (1995) 69.
[31] P.L. Richards, J. Appl. Phys. 76 (1994) 1.
[32] J. Clarke, P.L. Richards, N.-H. Yeh, Appl. Phys. Lett. 30 (1977) 664.
[33] P.W. Kruse, Semicond. Sci. Technol. 5 (1990) S229.
[34] A. Frenkel, Physica C 180 (1991) 251.
[35] I.A. Khrebtov, Sov. J. Opt. Technol. 58 (1991) 261.
[36] Z.M. Zhang, A. Frenkel, J. Supercond. 7 (1994) 871.
[37] H. Kraus, Supercond. Sci. Technol. 9 (1996) 827.
[38] A. Lee, P.L. Richards, S.W. Nam, B. Cabrera, K.D. Irwin, Appl. Phys. Lett. 69 (1996) 1801.

[39] K.D. Irwin, G.C. Hilton, D.A. Wollman, J.M. Martinis, Appl. Phys. Lett. 69 (1996) 1945.
[40] K.D. Irwin, Appl. Phys. Lett. 66 (1995) 1998.
[41] K.D. Irwin, S.W. Nam, B. Cabrera, B. Chugg, G.S. Park, R.P. Welty, J.M. Martinis, IEEE Trans. Appl. Supercond. 5 (1995) 690.
[42] D.A. Wollman, K.D. Irwin, G.C. Hilton, L.L. Dulcie, D.E. Newbury, J.M. Martinis, J. Microsc. 188 (1997) 196.
[43] J. Mather, Appl. Optics 21 (1982) 1125.
[44] F. Reif, Fundamentals of Statistical and Thermal Physics, Mc-Graw Hill, New York, 1965, pp. 213, 242.
[45] G.C. Hilton, J.M. Martinis, K.D. Irwin, N.F. Bergren, D.A. Willman, M.E. Huber, S. Deiker, S.W. Nam, IEEE Trans. Appl. Supercond. 11 (2001) 739.
[46] J.A. Chervenak, K.D. Irwin, E.N. Grossmann, J.M. Martinis, C.D. Reintsema, M.E. Huber, Appl. Phys. Lett. 74 (1999) 4043.
[47] M. Bravin, M. Bruckmayer, C. Bucci, S. Cooper, S. Giordano, F.v. Feilitzsch, J. Höhne, J. Jochum, V. Jörgens, R. Keeling, H. Kraus, M. Loidl, J. Lush, J. Macallister, J. Marchese, O. Meier, P. Meunier, U. Nagel, T. Nüssle, F. Pröbst, Y. Ramachers, M. Sarsa, J. Schnagl, W. Seidel, I. Sergeyev, M. Sisti, L. Stodolsky, S. Uchaikin, L. Zerle, Astroparticle Phys. 12 (1999) 107.
[48] G.C. Hilton, J.M. Martinis, D.A. Wollman, K.D. Irwin, L.L. Dulcie, D. Gerber, P.M. Gillevet, D. Twerenbold, Nature 391 (1998) 672.
[49] C. Hagmann, P.L. Richards, Cryogenics 35 (1995) 303.
[50] K. Uhlig, W. Hehn, Cryogenics 37 (1997) 279.